



**HAL**  
open science

## Sharp transition to strongly anomalous transport in unsaturated porous media

Andrés Velásquez-parra, Tomás Aquino, Matthias Willmann, Yves Méheust,  
Tanguy Le Borgne, Joaquín Jiménez-martínez

► **To cite this version:**

Andrés Velásquez-parra, Tomás Aquino, Matthias Willmann, Yves Méheust, Tanguy Le Borgne, et al..  
Sharp transition to strongly anomalous transport in unsaturated porous media. *Geophysical Research  
Letters*, 2022, 49 (3), pp.e2021GL096280. 10.1029/2021GL096280 . insu-03537085v1

**HAL Id: insu-03537085**

**<https://insu.hal.science/insu-03537085v1>**

Submitted on 20 Jan 2022 (v1), last revised 24 Feb 2022 (v2)

**HAL** is a multi-disciplinary open access archive for the deposit and dissemination of scientific research documents, whether they are published or not. The documents may come from teaching and research institutions in France or abroad, or from public or private research centers.

L'archive ouverte pluridisciplinaire **HAL**, est destinée au dépôt et à la diffusion de documents scientifiques de niveau recherche, publiés ou non, émanant des établissements d'enseignement et de recherche français ou étrangers, des laboratoires publics ou privés.

# Sharp transition to strongly anomalous transport in unsaturated porous media

Andrés Velásquez-Parra<sup>1,2</sup>, Tomás Aquino<sup>3</sup>, Matthias Willmann<sup>2</sup>, Yves  
Méheust<sup>3</sup>, Tanguy Le Borgne<sup>3</sup>, and Joaquín Jiménez-Martínez<sup>1,2</sup>

<sup>1</sup>Department of Water Resources and Drinking Water, Swiss Federal Institute of Aquatic Science and  
Technology, Eawag, Dübendorf, Switzerland

<sup>2</sup>Department of Civil, Environmental and Geomatic Engineering, ETH Zürich, Zürich, Switzerland

<sup>3</sup>Univ. Rennes, CNRS, Géosciences Rennes, UMR 6118, 35000 Rennes, France

## Key Points:

- The presence of an immiscible phase in porous media leads to an abrupt shift in the scaling of the liquid phase velocity distribution
- Dispersion is quasi-Fickian in saturated systems, but becomes quasi-ballistic under even slightly unsaturated conditions
- We predict flow and advective transport based on phase distribution and porous medium geometry

---

Corresponding author: Joaquín Jiménez-Martínez, joaquin.jimenez@eawag.ch /  
jjimenez@ethz.ch

This article has been accepted for publication and undergone full peer review but has not been through the copyediting, typesetting, pagination and proofreading process, which may lead to differences between this version and the [Version of Record](#). Please cite this article as doi: [10.1029/2021GL096280](https://doi.org/10.1029/2021GL096280).

This article is protected by copyright. All rights reserved.

## Abstract

The simultaneous presence of liquid and gas in porous media increases flow heterogeneity compared to saturated flows. However, the impact of saturation on flow and transport has so far remained unclear. The presence of gas in the pore space leads to flow reorganization. We develop a theoretical framework that captures the impact of that reorganization on pore-scale fluid velocities. Preferential flow is distributed spatially through a backbone and flow recirculation occurs in flow dead-ends. We observe, and predict theoretically, that this previously-identified flow structure induces a marked change in the scaling of the velocity probability density function compared to the saturated configuration, and a sharp transition to strongly anomalous transport. We develop a transport model using the continuous time random walk theory that predicts advective transport dynamics for all saturation degrees. Our results provide a new modeling framework linking phase heterogeneity to flow heterogeneity in unsaturated media.

## Plain Language Summary

The unsaturated zone, where water and air coexist in the pore space, extends between the soil surface and the groundwater level. Its pronounced structural heterogeneity induces complex flow patterns, which lead to rich solute transport behaviors. Inputs (precipitation) and outputs (evaporation and deep drainage) induce spatio-temporal variability in water saturation (i.e., fraction of the pore space occupied by water), which impacts flow, transport, and biochemical reactions. It has been observed that water-unsaturated conditions lead to a strong separation of flow in regions of high velocity, where most of the fluid is transported, and regions of low velocity. We identify the spatial distribution and size of the low-velocity regions as key control features on water flow and transport of dissolved chemical species, leading to transport behaviors that differ from those described by classical transport formulations. We use these findings to develop a theoretical framework that allows us to predict flow and advective transport under unsaturated conditions, based on parameters that describe the heterogeneity in phase distribution within the pore space and that are directly linked to the geometry of the system. These results represent a decisive step towards the prediction of fate and transport phenomena from structural properties in unsaturated porous media.

## 1 Introduction

Unsaturated porous media, where liquid and gas phases coexist, play a central role in a broad range of environmental and industrial applications, including contaminant transport (Lahav et al., 2010; Sebilo et al., 2013), artificial groundwater recharge (Bouwer, 2002), underground gas storage (Panfilov, 2010), radioactive waste disposal (Winograd, 1981), and energy storage (Barbier, 2002), among others. Previous studies have shown that under saturated conditions, i.e., for single-phase flow, structural heterogeneity in the solid phase is sufficient to induce anomalous transport (de Anna et al., 2013; Le Borgne et al., 2011; Holzner et al., 2015; Morales et al., 2017; Moroni et al., 2007; Kang et al., 2014; Stoop et al., 2019). This typically translates to early solute arrival and longer tailing at a given control plane, as well as non-Fickian scaling of spatial solute spreading (Berkowitz et al., 2006; Bijeljic et al., 2011), all features that cannot be described using classical transport formulations.

In unsaturated porous media, the presence of several immiscible or partially-miscible fluid phases in the pore space induces complex flow topologies, increasing flow tortuosity and resulting in more extreme high and low velocities (de Gennes, 1983; Jiménez-Martínez et al., 2017; Datta et al., 2013; Birkholzer & Tsang, 1997; Nützmänn et al., 2002; Wildenschild & Jensen, 1999). The consequences of this heterogeneity for solute transport properties remain controversial. Both an increase (Aziz et al., 2018; Bromly & Hinz, 2004; Haga et al., 1999; Padilla et al., 1999) and a decrease (Birkholzer & Tsang, 1997; Van-

66 derborgh & Vereecken, 2007) of dispersion with decreasing saturation have been reported.  
67 However, these studies have resorted to continuum/effective-scale theories, where the use  
68 of locally-averaged velocity values does not reflect the complexity of the pore-scale ve-  
69 locity field.

70 Here, we use images from millifluidic experiments and pore-scale numerical sim-  
71 ulations to derive a new theoretical framework linking medium structure parameters and  
72 saturation degree ( $S_w$ , fraction of the pore volume occupied by the liquid) to the prob-  
73 ability density function (PDF) of both flow rate through pore throats and velocities, and  
74 to anomalous transport dynamics. We identify a previously-unknown abrupt change in  
75 the velocity statistics, which become much broader even for low desaturations. Our the-  
76 ory is built on the partition of the pore space into two contrasting structures, a back-  
77 bone of preferential flow paths, and dead-end regions of low velocity. While the backbone/dead-  
78 end structure is known since the work of de Gennes (1983), dead-ends were simply as-  
79 sumed to have zero velocities, and its direct impact on velocity statistics remained un-  
80 known. Our theory elucidates the mechanisms leading to the observed transition and pre-  
81 dict the change exerted by the presence of dead-ends on the velocity PDF scaling for  
82 unsaturated systems, compared to fully saturated conditions. Using a continuous time  
83 random walk (CTRW) approach, parameterized according to the theoretical velocity PDFs,  
84 we predict a transition from quasi-Fickian to highly anomalous, quasi-ballistic transport  
85 in unsaturated systems, in agreement with resolved simulations.

## 86 2 Methods

### 87 2.1 Numerical Flow Simulations

88 We employ experimental images of a quasi two-dimensional (2D) porous medium  
89 characterizing the arrangement of two immiscible phases (water and air) under differ-  
90 ent  $S_w$  (1.00, 0.83, 0.77, and 0.71) (Jiménez-Martínez et al., 2017) and simulate flow at  
91 the pore scale. Experiments were performed for low capillary numbers, hence the air clus-  
92 ters (non-wetting phase) remain immobile (Tang et al., 2019). Under these conditions,  
93 variations in the viscosity of the non-wetting phase are not relevant. The dimensions of  
94 the system are 132 mm  $\times$  87 mm, and its thickness (vertical gap)  $h = 0.5$  mm. The av-  
95 erage pore throat width (shortest distance between grains)  $a_m = 1.17$  mm, and the mean  
96 pore size (meeting point of pore throats)  $\lambda = 1.85$  mm, leading to a porosity of 0.71,  
97 similar to that reported in other studies addressing 2D systems (Andrade, Jr. et al., 1997;  
98 Tallakstad et al., 2009).

99 We numerically simulate 2D steady-state Stokes flow, in which the flow of water  
100 around the solid grains and air bubbles is exclusively controlled by viscous dissipation.  
101 The effect of the third dimension on depth-averaged flow is introduced in the Stokes equa-  
102 tion through a Darcy-like term (Ferrari et al., 2015) representing the drag force exerted  
103 on the liquid by the upper and lower walls in the experimental configuration (Jiménez-  
104 Martínez et al., 2017). A constant flow rate of 1.375 mm<sup>3</sup>/s for the saturated case and  
105 0.277 mm<sup>3</sup>/s for the unsaturated cases is imposed at the inlet (Jiménez-Martínez et al.,  
106 2017). Atmospheric pressure is imposed at the outlet. We assign a no-slip boundary con-  
107 dition to solid-liquid interfaces and a slip boundary condition to liquid-gas interfaces,  
108 i.e., zero longitudinal stress is imposed along these interfaces rather than a zero veloc-  
109 ity (Kazemifar et al., 2016).

### 110 2.2 Particle Tracking Simulations

111 To investigate the consequences of our velocity analysis for advective transport, we  
112 also perform advective particle tracking simulations to allow for a numerical quantifi-  
113 cation of dispersion. We perform a flux-weighted injection of 10<sup>4</sup> particles along the in-  
114 let boundary of the porous medium, over an area with a length equal to the medium width

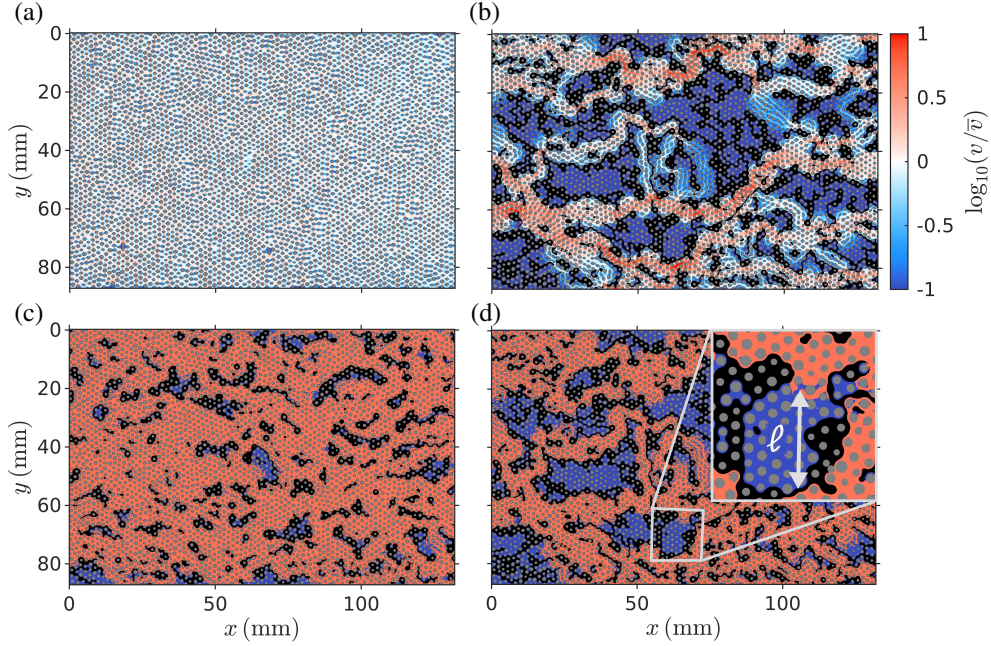


**Figure 1.** Velocity fields obtained from Stokes flow numerical simulations, displayed in terms of the velocity magnitude  $v$  normalized by its mean value  $\bar{v}$ , for (a)  $S_w = 1.00$  and (b)  $S_w = 0.71$ . The colorbar is common to subfigures (a) and (b), with red colors indicating high velocities and blue colors low velocities. Regions where  $\log_{10}(v/\bar{v}) \leq -1$  are shown in the darkest blue tone. The solid phase (circular obstacles) is shown in gray and air clusters in black. Subfigures (c) and (d) show the partition of the velocity field into two types of flow structures: (i) backbone or preferential paths, depicted in red, and (ii) dead-end regions of low velocity, depicted in blue, for  $S_w = 0.83$  and  $S_w = 0.71$ , respectively. The inset in subfigure (d) depicts the geometry of a dead-end region, with  $\ell$  representing the dead-end region's depth.

115 in the  $y$ -direction and a width equal to the average grain size (i.e., 0.83 mm) along the  
 116  $x$ -axis. Particle positions are tracked isochronically over fixed time steps  $\Delta t$  ( $t$ -Lagrangian  
 117 sampling). For  $S_w = 1.00$ ,  $\Delta t = 0.05 t_a$ , where  $t_a = \lambda/\bar{v}$  is the advective time over  
 118 the mean pore size  $\lambda$  at the mean velocity  $\bar{v}$ . For the unsaturated cases,  $\Delta t$  ranges be-  
 119 tween  $0.021 t_a$  and  $0.029 t_a$ . A 100 times finer time discretization is introduced at early  
 120 times to improve resolution in the ballistic dispersion regime.

### 121 3 Prediction of Unsaturated Flow Distribution

#### 122 3.1 Impact of Saturation on Flow Velocities

123 While the simulated velocity fields exhibit limited variability under saturated condi-  
 124 tions (Figure 1a), the flow heterogeneity is strongly enhanced in the unsaturated case  
 125 (Figure 1b). The introduction of air induces a partition of the flow field into two flow  
 126 structures (de Gennes, 1983): a backbone of preferential flow paths, and dead-end re-  
 127 gions (velocity is non-zero (Jiménez-Martínez et al., 2017, 2015)) that branch out from  
 128 the backbone (Figure 1c and 1d). For the Eulerian velocity PDF  $p_E(v)$ , this reorgani-  
 129 zation of flow compared to the saturated case leads to an increase in the probability of  
 130 low velocities (Figure 2a), as they are not only encountered close to the solid-liquid in-  
 131 terfaces but also within dead-end regions (Figure 1b). This is described by the sharp tran-  
 132 sition from a plateau for  $S_w = 1.00$  to a power-law-like behavior for  $S_w < 1.00$ . High

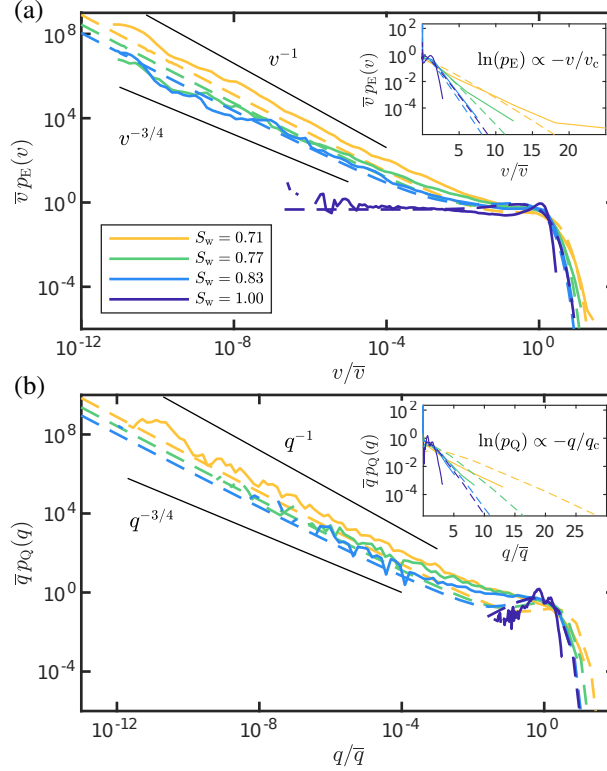


**Figure 2.** Numerical (continuous lines) and predicted (dashed lines) PDFs for (a) Eulerian velocities and (b) pore flow rates, normalized by their respective average values  $\bar{v}$  and  $\bar{q}$ , for  $S_w = 1.00, 0.83, 0.77,$  and  $0.71$ . The log-log scale highlights the scaling of low magnitudes; the power law scalings are shown for visual reference. Semi-log insets highlight the exponential behavior at high magnitudes.

133 velocities follow an exponential trend, in agreement with existing literature (Datta et al.,  
134 2013), and can be characterized by a saturation-dependent characteristic velocity  $v_c$ .

135 We partition the flow field into backbone and dead-end regions (Figure 1c and 1d)  
136 by selecting a velocity threshold at the transition between the power-law and exponen-  
137 tial velocity regimes. Results suggest a more accentuated flow separation with lower sat-  
138 uration, where dead-end regions increase both in size and number as  $S_w$  decreases, and  
139 where the dead-end area PDF  $p_A$  decays as a power-law (Figure 3). Note that previous  
140 studies in 2D porous media have analyzed air cluster area distributions, rather than fluid  
141 dead-end area distributions, and found a power-law behavior with an exponential cut-  
142 off at large cluster sizes (Jiménez-Martínez et al., 2017; Tallakstad et al., 2009).

### 143 3.2 Theoretical Flow Model

144 To derive a theoretical framework for  $p_E(v)$ , we first consider the local flow rate  
145 through a pore throat, or pore flow rate  $q$ . It is computed by integrating flow velocities  
146 over the cross section of the pore throat. For all unsaturated conditions, the PDF of pore  
147 flow rates over the ensemble of throats  $p_Q(q)$  shows a scaling similar to that of  $p_E(v)$  for  
148 both low and high magnitudes (Figure 2a). However, for  $S_w = 1.00$ ,  $p_Q(q)$  increases  
149 with  $q$  at low values instead of the plateau observed for  $p_E(v)$ . For  $S_w = 1.00$ ,  $p_Q(q)$   
150 is well captured by the flow rate PDF in the backbone  $p_Q^b$ , which follows a gamma dis-

tribution,

$$p_Q^b(q) = \frac{qe^{-q/q_c}}{q_c^2}, \quad (1)$$

where the saturation-dependent characteristic flow rate  $q_c$  controls the exponential high-flow tailing. This is consistent with the random aggregation model of Alim et al. (2017), based on the random splitting and merging of flow throughout the pore network (Coppersmith, 1996).

To model  $p_Q(q)$  and  $p_E(v)$  for  $S_w < 1.00$ , we quantify the flow statistics in backbone ( $p_Q^b$ ) and dead-end ( $p_Q^d$ ) regions. We first determine the ratio  $f$  of the area occupied by dead-end regions to the total area of the pore space (e.g., 0.2601 for  $S_w = 0.71$ , refer to Supplementary Material for the remaining  $S_w$ ). We express  $p_Q(q)$  as

$$p_Q(q) = fp_Q^d(q) + (1 - f)p_Q^b(q). \quad (2)$$

Next, we determine  $p_Q^d$ . Simulation data suggest that flow-rate magnitudes within dead-end regions decay exponentially with depth  $0 \leq z \leq \ell$  (see Supplementary Material), up to the total depth  $\ell$  of the dead-end region, which extends from the contact with the backbone to the far liquid-gas boundary (see inset in Figure 1d). Such exponential decay is consistent with the fundamental solutions of the Laplace equation for the propagation within the dead-end of the pressure perturbation applied from the boundary with the backbone (Bland, 1965). We expect macroscopic pressure gradients within dead-ends regions to obey a Laplace equation resulting from Darcy's law (Whitaker, 1986). We thus approximate the flow rate decay along the depth as

$$q_d(z|\ell) \approx q_0 e^{-z/a_m} H(\ell - z), \quad (3)$$

where  $q_0 = q_d(0|\ell)$  is the flow rate at the contact with the backbone and  $H$  is the Heaviside step function. Since this flow rate profile is monotonically decreasing, the associated PDF for a given  $q_0$  and  $\ell$  can be computed as (Aquino & Le Borgne, 2021)

$$p_Q^d(q|\ell, q_0) = \left( \ell \frac{dq_d(z|\ell)}{dz} \Big|_{z=z_q(q)} \right)^{-1}, \quad (4)$$

where  $z_q(q)$  is the point at which the flow has a given value  $q$ , i.e.,  $q_d[z_q(q)|\ell] = q$ . Thus, inverting Eq. (3) for depth as a function of flow rate, computing  $dq_d(z|\ell)/dz$ , and substituting, Eq. (4) becomes

$$p_Q^d(q|\ell, q_0) = \frac{a_m}{\ell q} H(q_0 - q) H(q - q_0 e^{-\ell/a_m}), \quad (5)$$

for the dead-end flow-rate PDF  $p_Q^d(\cdot|\ell, q_0)$ , given maximum depth  $\ell$  and flow rate  $q_0 = q_d(0|\ell)$  at the entrance. Taking  $q_0$  to be distributed according to Eq. (1) and averaging over the latter, we can now express the flow rate PDF in dead-ends given  $\ell$  as

$$p_Q^d(q|\ell) = \int_0^\infty dq_0 p_Q^d(q|\ell, q_0) p_Q^b(q_0), \quad (6)$$

which after computing the integral leads to

$$p_Q^d(q|\ell) = \frac{a_m}{\ell q_c q} \left[ e^{-q/q_c} (q + q_c) - \exp\left(-\frac{e^{\ell/a_m} q}{q_c}\right) (e^{\ell/a_m} q + q_c) \right]. \quad (7)$$

By approximating  $\ell \approx \sqrt{A}$ , with  $A$  the dead-end area, and averaging over areas, we obtain an expression for the PDF of dead-end flow rates,

$$p_Q^d(q) \approx \int_0^\infty dA p_Q^d(q|\sqrt{A}) p_A(A). \quad (8)$$

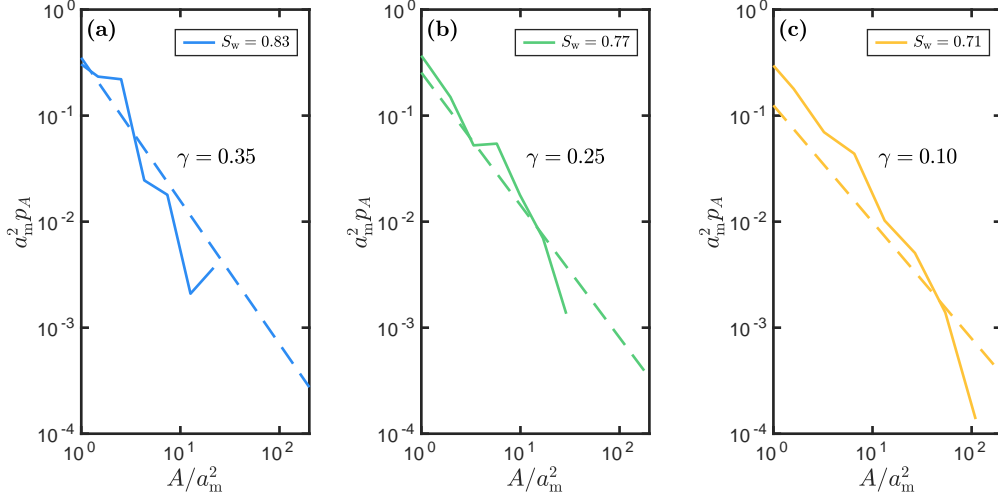


**Figure 3.** PDF of the dead-end areas  $p_A$  for (a)  $S_w = 0.83$ , (b)  $S_w = 0.77$ , and (c)  $S_w = 0.71$ . For all three cases,  $p_A$  is well approximated by a Pareto PDF (Eq. (9)) describing power-law decay. Corresponding values of the fitting parameter  $\gamma$  describing a power law decay  $\propto A^{-1-\gamma}$ , which decreases with decreasing liquid phase saturation, are also shown. Quantities are non-dimensionalized with respect to the area  $a_m^2$  associated with the average pore-throat aperture.

The PDF  $p_A$  of dead-end areas, defined for a given flow field such that  $p_A(A) dA$  is the probability of a uniformly randomly chosen dead-end region to have area in an infinitesimal neighborhood  $dA$  of  $A$ , is shown in Figure 3 for each unsaturated flow field. The area PDFs were determined based on the flow field partitions, as shown in Figure 1 for  $S_w = 0.83$  and  $S_w = 0.71$ . We approximate  $p_A$  by a Pareto PDF,

$$p_A(A) = \frac{\gamma}{a_m^2} \left( \frac{A}{a_m^2} \right)^{-1-\gamma} H(A - a_m^2), \quad (9)$$

where the exponent  $\gamma$  decreases with decreasing  $S_w$ , indicating broader dead-end area variability. The approximations thus obtained are plotted as dashed lines in Figure 3. We consider the minimum area of a dead-end region to be equal to the area of one pore throat, approximated as  $a_m^2$ .

We can now expand the integrand in Eq. (8) using Eq. 9, obtaining

$$p_Q^d(q) \approx \int_0^\infty dA \frac{a_m}{q_c \sqrt{A}} e^{-q/q_c} p_A(A). \quad (10)$$

Computing this integral, and combining it with the expression for  $p_Q^b(q)$  (Eq. (1)) in Eq. (2), we deduce an expression for  $p_Q(q)$ . For  $q \ll q_c$ , the latter is controlled by the dead-end contribution as long as  $f \neq 0$ , corresponding to  $S_w < 1.00$ . Notice also that the nested exponential in Eq. (7) varies rapidly from zero to unity around  $q = q_c e^{-\ell/a_m}$ , so that it is well approximated by a cutoff for  $A \approx \ell^2 > [a_m \ln(q_c/q)]^2$ . This leads to

$$\begin{aligned} p_Q^d(q) &\approx \int_0^\infty dA \frac{a_m}{q_c \sqrt{A}} \left[ 1 - H \left( \left[ a_m \ln \left( \frac{q_c}{q} \right) \right]^2 - A \right) \right] p_A(A), \\ &\approx \frac{2\gamma}{q(1+2\gamma)} \left[ \ln \left( \frac{q_c}{q} \right) \right]^{-1-2\gamma}, \quad q \ll q_c, \end{aligned} \quad (11)$$

209 which, combined with Eqs. (1) and (2), leads to

$$210 \quad p_Q(q) \approx \frac{2\gamma f}{q(1+2\gamma)} \left[ \ln \left( \frac{q_c}{q} \right) \right]^{-1-2\gamma}. \quad (12)$$

211 Thus, our model predicts that for  $S_w < 1.00$ ,  $p_Q(q)$  scales for low flow rates as  
 212 a power law,  $q^{-1}$ , corrected by a logarithmic factor, raised to a power controlled by  $p_A(A)$   
 213 through the exponent  $\gamma$ . In the particular case  $f = 0$ , i.e.,  $S_w = 1.00$ , Taylor expansion  
 214 of  $p_Q^b$  (Eq. (1)) for low  $q$  leads to  $p_Q(q) \approx q/q_c^2$ , linear in  $q$ . Proceeding similarly  
 215 for  $q \gtrsim q_c$ , for which we must consider contributions from both  $p_Q^b(q)$  and  $p_Q^d(q)$ , we  
 216 obtain the exponential decay

$$217 \quad p_Q(q) \approx \left[ \frac{2\gamma f}{1+2\gamma} + (1-f) \frac{q}{q_c} \right] \frac{e^{-q/q_c}}{q_c}. \quad (13)$$

218 We now turn our attention to  $p_E(v)$ . It results from the combined effect of  $p_Q(q)$   
 219 and the intra-throat variability arising from the local velocity profile within each throat.  
 220 Thus, these two PDFs are related by

$$221 \quad p_E(v) = \int_0^\infty dq p_Q(q) p_E(v|q), \quad (14)$$

222 where  $p_E(\cdot|q)$  is the PDF of velocities associated with a pore throat characterized by  $q$ .  
 223 Since pore throat widths are comparable in size to the channel thickness  $h$ , we consider  
 224 the impact of this third dimension on the intra-pore, depth-averaged 2D velocity profile.  
 225 The latter differs from the parabolic profile expected in a purely-2D scenario (see  
 226 Supplementary Material for plot of velocity profiles across the system). By approximat-  
 227 ing the pore throat as a cuboid channel of width  $a_m$  and thickness  $h$ , we express the ve-  
 228 locity profile for Stokes flow over the channel thickness  $h$  as a series in the form (Bruus,  
 229 2008)

$$230 \quad v_x(y, z) = \frac{4h^2 \Delta p}{\pi^3 \mu L} \sum_{n, \text{odd}} \frac{1}{n^3} \left[ 1 - \frac{\cosh(n\pi \frac{y}{h})}{\cosh(n\pi \frac{a_m}{2h})} \right] \sin \left( n\pi \frac{z}{h} \right), \quad (15)$$

231 where  $\mu$  is the viscosity of the liquid (wetting) phase,  $\Delta p$  is the pressure difference across  
 232 the cuboid channel of length  $L$ , and the sum extends over odd values of  $n$  as indicated.  
 233 Here we have set a local coordinate system at each pore throat, with  $x$  representing the  
 234 local mean flow direction, the throat width running parallel to  $y$ , and  $z$  running along  
 235 the channel thickness. Averaging this function over  $z$  values between 0 and  $h$ , we obtain

$$236 \quad \langle v_x(y, z) \rangle_z = \frac{8h^2 \Delta p}{\pi^4 \mu L} \sum_{n, \text{odd}} \frac{1}{n^4} \left[ 1 - \frac{\cosh(n\pi \frac{y}{h})}{\cosh(n\pi \frac{a_m}{2h})} \right], \quad (16)$$

237 where  $\langle \cdot \rangle$  denotes the mean value. Given the low variability of pore-throat sizes across  
 238 the medium, we approximate throat widths by their average value  $a_m$ . For the dimen-  
 239 sions of our porous medium (thickness  $h$  and average throat width  $a_m$ ), this series is gov-  
 240 erned by its first term, reducing the expression to

$$241 \quad \langle v_x(y, z) \rangle_z \approx \frac{h^2 \Delta p}{2\pi^4 \mu L} \left[ 1 - \frac{\cosh(2\pi \frac{y}{h})}{\cosh(\pi \frac{a_m}{h})} \right]. \quad (17)$$

242 The Eulerian velocity PDF associated with the velocity profile across a pore throat with  
 243 local flow rate  $q$  is then (see Supplementary Material for further details)

$$244 \quad p_E(v|q) = \frac{2h}{\pi a_m v_{\max}(q)} \frac{(C-1)H[v_{\max}(q) - v]}{\sqrt{[C - (C-1)v/v_{\max}(q)]^2 - 1}}, \quad (18)$$

245 where  $C = \cosh[\pi a_m/(2h)]$ , and  $v_{\max}(q) = \alpha q/(ha_m)$  is the maximum velocity within  
 246 the pore throat, with

$$247 \quad \alpha = 2 \left( 1 + \coth \left( \frac{\pi a_m}{4h} \right) \left[ \coth \left( \frac{\pi a_m}{4h} \right) - \frac{4h}{\pi a_m} \right] \right)^{-1}. \quad (19)$$

248 For  $S_w = 1.00$ , the integral in Eq. (14) can then be approximated for  $v \ll v_c$  and  
 249  $v \gtrsim v_c = q_c/(a_m h)$ , respectively, by using Eq. (1), as

$$250 \quad p_E(v) \approx \frac{2h}{\pi a_m \alpha v_c} \tanh \left( \frac{\pi a_m}{4h} \right), \quad (20a)$$

$$251 \quad p_E(v) \approx \frac{2h}{\alpha a_m v_c} \sinh \left( \frac{\pi a_m}{4h} \right) \sqrt{\frac{v}{\pi \alpha v_c}} e^{-\frac{v}{\alpha v_c}}. \quad (20b)$$

252 Equation (20a) describes a low-velocity plateau, while Eq. (20b) encodes exponential tail-  
 253 ing at large velocities.

254 For  $S_w < 1.00$ , the previous derivation holds for the backbone component. Sim-  
 255 ilar to  $p_Q(q)$ ,  $p_E(v)$  for  $v \ll v_c$  is dominated by the dead-end regions, while for  $v \gtrsim$   
 256  $v_c$  the contribution of both backbone and dead-ends matters. The low-velocity behav-  
 257 ior is controlled by low flow rates. For small  $q$ ,  $p_E(v|q)$  becomes arbitrarily narrow, be-  
 258 cause the maximum velocity is linear in  $q$ , see Eq. (18). Accordingly,  $p_E(v)$  is well ap-  
 259 proximated for low  $v$  by setting  $p_E(v|q) \approx \delta[v - q/(ha_m)]$  in Eq. (14), where  $\delta(\cdot)$  is the  
 260 Dirac delta, and by using Eq. (12) for  $p_Q(q)$ . We obtain, for  $v \ll v_c$ ,  
 261

$$262 \quad p_E(v) \approx \frac{2\gamma f}{v(1+2\gamma)} \left[ \ln \left( \frac{v_c}{v} \right) \right]^{-1-2\gamma}. \quad (21)$$

263 Analogously, for  $v \gtrsim v_c$ ,  $p_E(v)$  can be computed using Eq. (13) for  $p_Q(q)$ , and Tay-  
 264 lor expanding Eq. (18) for  $v \approx v_{\max}(q)$ , which leads to

$$265 \quad p_E(v) \approx \left[ \frac{2\gamma f}{1+2\gamma} \sqrt{\frac{\alpha v_c}{v}} + (1-f) \sqrt{\frac{v}{\alpha v_c}} \right] \frac{C_* e^{-\frac{v}{\alpha v_c}}}{\alpha v_c}, \quad (22)$$

266 where  $C_* = 2h \sinh(\pi a_m/4h)/(\sqrt{\pi} a_m)$ . Note that for large  $h$  values compared to  $a_m$ ,  
 267 Eqs. (20a)–(22) reduce to expressions that correspond to those obtained under the as-  
 268 sumption of a Poiseuille velocity profile (fully-2D case) (see Supplementary material for  
 269 a complete mathematical deduction).

270 Figure 2 shows the predictions (dashed lines) for both  $p_Q(q)$  and  $p_E(v)$ . The model  
 271 successfully captures the different regimes and scaling variation for the various  $S_w$ . The  
 272 low-velocity plateau for  $S_w = 1.00$  is also captured. The results shown here correspond  
 273 to numerical computation of the full theoretical PDFs according to Eqs. (1), (2), (8), and (14).  
 274 Further details on the regime scalings and parameter values can be found in the Sup-  
 275 plementary Material.

## 276 4 Prediction of Advective Transport

277 Using the results of the particle tracking simulations (see Section 2.2), we compute  
 278 (advective) dispersion  $\sigma_x^2(t)$ , as a function of time  $t$ , as the variance of longitudinal par-  
 279 ticle positions. Lower saturation induces larger particle dispersion due to the increased  
 280 velocity heterogeneity, as discussed above. At early times, a ballistic regime,  $\sigma_x^2 \sim t^2$   
 281 is observed in Figure 4 for all  $S_w$ , which then transitions to an asymptotic superdiffu-  
 282 sive regime. The crossover time between the ballistic and asymptotic regimes is also larger  
 283 for smaller  $S_w$ , i.e., the Lagrangian correlation length  $\zeta_x$  of velocities along the mean flow  
 284 direction increases with decreasing saturation (refer to Supplementary material for cor-  
 285 relation plots).

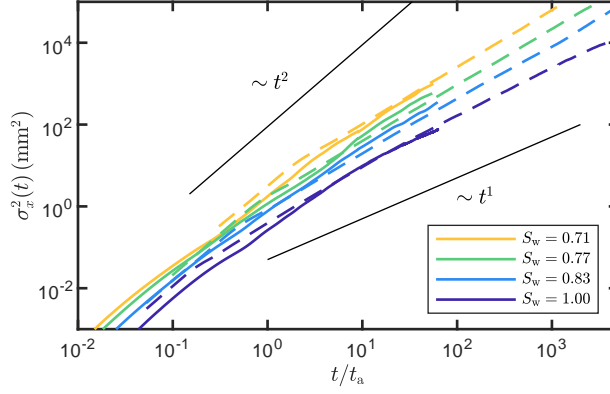


**Figure 4.** Advective dispersion  $\sigma_x^2$  in time for  $S_w = 1.00, 0.83, 0.77,$  and  $0.71$ . Time is normalized by the advective time  $t_a = \lambda/\bar{v}$  over the mean pore size  $\lambda$ . The plot compares  $\sigma_x^2$  from the particle tracking analysis (continuous lines) with  $\sigma_x^2$  from a CTRW approach computed using the predicted velocity PDF  $p_E(v)$  (dashed lines). Scalings for a ballistic ( $\sigma_x^2 \sim t^2$ ) and a Fickian ( $\sigma_x^2 \sim t^1$ ) regime are also displayed for reference.

286 To develop a transport modeling framework that links the dispersion dynamics to  
 287 hydrodynamics, we employ a CTRW approach (Berkowitz et al., 2006; Dentz et al., 2016;  
 288 Cortis & Berkowitz, 2004). The CTRW framework used here models transport in terms  
 289 of Lagrangian particles taking fixed spatial steps of length  $\zeta_x$  along the mean flow di-  
 290 rection (*s*-Lagrangian sampling). Particle velocities remain constant over a step and are  
 291 assumed to fully decorrelate between steps. They are sampled independently in each step  
 292 from the *s*-Lagrangian velocity distribution, which is given by the flux-weighted  $p_E(v)$ ,  
 293  $p_s(v) = vp_E(v)/\bar{v}$  (Dentz et al., 2016). This approach captures the intermittent nature  
 294 of the *t*-Lagrangian velocity signal through the distributed waiting times to cross the fixed  
 295 distance  $\zeta_x$ .

296 To assess the applicability of our theoretical model to predict advective transport,  
 297 we employ  $p_s(v)$  defined from the predicted  $p_E(v)$  (dashed lines in Figure 2a) in the CTRW  
 298 description. Figure 4 shows  $\sigma_x^2$  computed from the resulting CTRW for each  $S_w$  (dashed  
 299 lines), together with  $\sigma_x^2$  computed from the particle tracking simulations. Dispersion is  
 300 well predicted over both the ballistic and superdiffusive regimes, and so the impact of  
 301  $S_w$  on the temporal scaling. A slight overestimation of early-time dispersion is visible  
 302 for  $S_w = 1.00$ , which might be explained by the assumption of full velocity decorrela-  
 303 tion beyond  $\zeta_x$ . Late-time dispersion is well captured in all cases, exhibiting more pro-  
 304 nounced superdiffusive behavior for  $S_w < 1.00$ . Overall, these results support the suit-  
 305 ability of both our theoretical description of velocity statistics and the CTRW to pre-  
 306 dict advective transport in unsaturated porous media, representing a major step towards  
 307 predicting solute transport in such systems from the sole knowledge of the medium's ge-  
 308 ometry.

309 The CTRW model presented here provides a theoretical framework to quantify the  
 310 relationship between dispersive scalings and velocity variability. In particular, the late-  
 311 time scaling is controlled by the low-velocity behavior of  $p_E(v)$ . If  $p_E(v)$  exhibits power-  
 312 law decay near  $v = 0$ ,  $p_E(v) \sim v^{-\theta}$  with  $0 < \theta < 1$ , late-time dispersion scales like  
 313  $\sigma_x^2 \sim t^{1+\theta}$  (Dentz et al., 2016), between the Fickian and ballistic limits  $\sigma_x^2 \sim t$  and  
 314  $\sigma_x^2 \sim t^2$ . The scalings found here for saturated and unsaturated conditions correspond  
 315 to two contrasting edge-cases. Under saturated conditions,  $\theta = 0$  (Eq. (20a)), which  
 316 leads to logarithmically-enhanced Fickian dispersion (Dentz et al., 2016). Note that pure  
 317 power-law decay characterized by  $\theta \geq 1$  is not integrable near  $v = 0$ . In this sense,

318 unsaturated conditions are characterized by maximal variability of low velocities, described  
 319 by logarithmic corrections to power-law decay with  $\theta = 1$  (Eq. (21)). This leads to logarithmically-  
 320 inhibited ballistic dispersion. In light of these considerations, along with the fact that  
 321 the unsaturated  $p_E(v)$  is broader than for the saturated case (Figure 2), the apparent  
 322 power-law scalings in Figure 4 vary slowly with time, as logarithmic corrections and the  
 323 effect of progressively lower velocities come into play. A rigorous derivation of asymp-  
 324 totic dispersion scalings is beyond the scope of this work and will be presented elsewhere.

## 325 5 Conclusions and Outlook

326 Here we have presented a new theoretical framework for the prediction of pore-scale  
 327 flow PDFs and advective transport capturing the impact of liquid-phase saturation. Re-  
 328 sults reveal that the introduction of an immiscible gas phase leads to a shift in the scal-  
 329 ing of the velocity PDFs that induces a sharp transition to strongly anomalous trans-  
 330 port. Under saturated conditions, dispersion is quasi-Fickian. In contrast, even under  
 331 slightly unsaturated conditions, dispersion becomes quasi-ballistic. In practice, this su-  
 332 perdiffusive dispersion behavior is sustained until low-velocity cutoffs introduced by ad-  
 333 ditional processes, such as diffusion, become relevant. The long-term residence time of  
 334 a particle in a dead-end region is eventually controlled by molecular diffusion, effectively  
 335 cutting off extreme slow velocities (de Gennes, 1983). While in the presence of diffusion  
 336 the transport is thus always asymptotically Fickian at sufficiently late times, the disper-  
 337 sive scalings related to the velocity variability remain relevant over significant time scales.  
 338 Our CTRW formulation also opens the door to the quantification of nontrivial scalings  
 339 of dispersion (Bijeljic & Blunt, 2006; Aquino & Le Borgne, 2021).

340 The theoretical formulation developed here successfully predicts flow and velocity  
 341 PDFs based only on a small set of parameters, which reflect characteristics of the porous  
 342 medium (average pore throat width  $a_m$  and thickness  $h$ ), the relative occupancy of back-  
 343 bone and dead-ends in the system (power-law tailing exponent  $\gamma$  and ratio of dead-end  
 344 area to total pore-space area  $f$ ), and flow properties (correlation length of longitudinal  
 345 velocities  $\zeta_x$  and tortuosity  $\chi$ , along with the characteristic flow rate  $q_c$ , used to deter-  
 346 mine the characteristic velocity  $v_c = q_c/(ha_m)$ ). While the values of these parameters  
 347 depend on properties such as porosity and liquid phase saturation, we expect the uncov-  
 348 ered transition in the velocity PDF and its impact on transport scaling properties to be  
 349 robust.

350 We expect the power-law dead-end area distribution to hold for (quasi-)2D systems,  
 351 independently of the detailed pore geometry. In particular, it holds for fully 2D systems,  
 352 and so does the spatial distribution of pore flow rates in dead-end regions (Eq. (3)), pro-  
 353 viding good predictions for  $h/a_m \gg 1$ . In addition, we also expect it to persist in 3D  
 354 systems, as is known to happen for both wetting and non-wetting phase cluster size dis-  
 355 tributions (Iglauer et al., 2010, 2012; Scheffer et al., 2021). These authors also report this  
 356 behavior for wetting phase saturation degrees lower than 0.71, which we could not achieve  
 357 in the present study, as they would approach the percolation threshold for the experi-  
 358 mental medium. However, following previous works that report a decrease in dispersiv-  
 359 ity once the system is desaturated below the so-called critical saturation (Raouf & Has-  
 360 sanizadeh, 2013), we hypothesize a decrease in the broadness of the velocity distribution  
 361 through an increase in the dead-end area-PDF exponent  $\gamma$  for saturation degrees below  
 362 that critical saturation. In addition, although the present study considers a high poros-  
 363 ity (0.71), the distribution of non-wetting-phase cluster sizes still exhibits power-law be-  
 364 havior for porosity values as low as 0.11 (Iglauer et al., 2010, 2012; Scheffer et al., 2021).  
 365 The effect of broader pore size variability (de Anna et al., 2017) under unsaturated con-  
 366 ditions remains an important open question. Note, however, that even if a different func-  
 367 tional dependency were observed for the dead-end area PDF, our new theoretical frame-  
 368 work provides the means to quantify its impact on flow velocity distributions and trans-  
 369 port. Furthermore, the upscaling of flow and transport presented here is a first step to-

370 wards theoretical assessment of mixing and chemical reactions in unsaturated porous me-  
371 dia, which are essential processes for the analysis and optimization of environmental and  
372 industrial systems.

### 373 Acknowledgments

374 A.V.-P. and J.J.-M. gratefully acknowledge the financial support from the Swiss  
375 National Science Foundation (SNF, grant Nr. 200021 178986). T.A. is supported by a  
376 Marie Skłodowska Curie Individual Fellowship, funded by the European Unions Hori-  
377 zon 2020 research and innovation program under the project *ChemicalWalks* 838426. Y.M.  
378 and T.L.B. acknowledge funding from ERC project *ReactiveFronts* 648377.

### 379 6 Open Research

380 The raw experimental images for all four saturation degrees, employed in the nu-  
381 merical simulations, are available under open access in Jiménez-Martínez et al. (2017)  
382 (<https://doi.org/10.1002/2016WR019849>).

### 383 References

- 384 Alim, K., Parsa, S., Weitz, D. A., & Brenner, M. P. (2017). Local pore size corre-  
385 lations determine flow distributions in porous media. *Physical Review Letters*,  
386 *119*(14), 144501. doi: 10.1103/PhysRevLett.119.144501
- 387 Andrade, Jr., J. S., Almeida, M. P., Mendes Filho, J., Havlin, S., Suki, B., &  
388 Stanley, H. E. (1997). Fluid flow through porous media: The role of stag-  
389 nant zones. *Physical Review Letters*, *79*(20), 3901–3904. doi: 10.1103/  
390 PhysRevLett.79.3901
- 391 Aquino, T., & Le Borgne, T. (2021). The diffusing-velocity random walk: a spatial-  
392 markov formulation of heterogeneous advection and diffusion. *Journal of Fluid*  
393 *Mechanics*, *910*, A12. doi: 10.1017/jfm.2020.957
- 394 Aziz, R., Joekar-Niasar, V., & Martinez-Ferrer, P. (2018). Pore-scale insights into  
395 transport and mixing in steady-state two-phase flow in porous media. *Internat-*  
396 *ional Journal of Multiphase Flow*, *109*, 51–62. doi: 10.1016/j.ijmultiphaseflow  
397 .2018.07.006
- 398 Barbier, E. (2002). Geothermal energy technology and current status: An overview.  
399 *Renewable and Sustainable Energy Reviews*, *6*(1-2), 3–65. doi: 10.1016/S1364  
400 -0321(02)00002-3
- 401 Berkowitz, B., Cortis, A., Dentz, M., & Scher, H. (2006). Modeling Non-fickian  
402 transport in geological formations as a continuous time random walk. *Reviews*  
403 *of Geophysics*, *44*(2), 1–49. doi: 10.1029/2005RG000178
- 404 Bijeljic, B., & Blunt, M. J. (2006). Pore-scale modeling and continuous time random  
405 walk analysis of dispersion in porous media. *Water Resources Research*, *42*(1).  
406 doi: 10.1029/2005WR004578
- 407 Bijeljic, B., Rubin, S., Scher, H., & Berkowitz, B. (2011). Non-Fickian transport in  
408 porous media with bimodal structural heterogeneity. *Journal of Contaminant*  
409 *Hydrology*, *120-121*, 213–221. doi: 10.1016/j.jconhyd.2010.05.007
- 410 Birkholzer, J., & Tsang, C.-f. (1997). Solute channeling in unsaturated heteroge-  
411 neous porous media. *Water Resources Research*, *33*(10), 2221–2238. doi: 10  
412 .1029/97WR01209
- 413 Bland, D. R. (1965). *Solutions of Laplace's Equation*. Plymouth: Routledge.
- 414 Bouwer, H. (2002). Artificial recharge of groundwater: Hydrogeology and engineer-  
415 ing. *Hydrogeology Journal*, *10*(1), 121–142. doi: 10.1007/s10040-001-0182-4
- 416 Bromly, M., & Hinz, C. (2004). Non-Fickian transport in homogeneous unsatu-  
417 rated repacked sand. *Water Resources Research*, *40*, 1–12. doi: 10.1029/

- 2003WR002579
- 418 Bruus, H. (2008). *Theoretical microfluidics - oxford master series in condenser mat-*  
419 *ter physics*. Oxford University Press.
- 420  
421 Coppersmith, D. (1996). *Advances in cryptology - eurocrypt '96, lecture notes in*  
422 *computer science* (Vol. 1070). Springer, Berlin.
- 423 Cortis, A., & Berkowitz, B. (2004). Anomalous Transport in “Classical” Soil and  
424 Sand Columns. *Soil Science Society of America Journal*, 68(5), 1539–1548.  
425 doi: 10.2136/sssaj2004.1539
- 426 Datta, S. S., Chiang, H., Ramakrishnan, T. S., & Weitz, D. A. (2013). Spa-  
427 tial fluctuations of fluid velocities in flow through a three-dimensional  
428 porous medium. *Physical Review Letters*, 111(6), 064501. doi: 10.1103/  
429 PhysRevLett.111.064501
- 430 de Anna, P., Le Borgne, T., Dentz, M., Tartakovsky, A. M., Bolster, D., & Davy,  
431 P. (2013). Flow intermittency, dispersion, and correlated continuous time  
432 random walks in porous media. *Physical Review Letters*, 110(18), 184502. doi:  
433 10.1103/PhysRevLett.110.184502
- 434 de Anna, P., Quaipe, B., Biros, G., & Juanes, R. (2017). Prediction of the low-  
435 velocity distribution from the pore structure in simple porous media. *Physical*  
436 *Review Fluids*, 2(12), 124103. doi: 10.1103/PhysRevFluids.2.124103
- 437 de Gennes, P. G. (1983). Hydrodynamic dispersion in unsaturated porous media.  
438 *Journal of Fluid Mechanics*, 136, 189–200. doi: 10.1007/978-1-4757-2558-2\_2
- 439 Dentz, M., Kang, P. K., Comolli, A., Le Borgne, T., & Lester, D. R. (2016). Con-  
440 tinuous time random walks for the evolution of Lagrangian velocities. *Physical*  
441 *Review Fluids*, 1(7), 074004. doi: 10.1103/PhysRevFluids.1.074004
- 442 Ferrari, A., Jiménez-Martínez, J., Le Borgne, T., Meheust, Y., & Lunati, I.  
443 (2015). Challenges in modeling unstable two-phase flow experiments in  
444 porous micromodels. *Water Resources Research*, 51, 1381–1400. doi:  
445 10.1002/2014WR016384
- 446 Haga, D., Niihori, Y., & Chida, T. (1999). Hydrodynamic dispersion and mass  
447 transfer in unsaturated flow. *Water Resources Research*, 35(4), 1065–1077. doi:  
448 10.1029/1998WR900111
- 449 Holzner, M., Morales, V. L., Willmann, M., & Dentz, M. (2015). Intermittent La-  
450 grangian velocities and accelerations in three-dimensional porous medium flow.  
451 *Physical Review E*, 92(1), 013015. doi: 10.1103/PhysRevE.92.013015
- 452 Iglauer, S., Favretto, S., Spinelli, G., Schena, G., & Blunt, M. J. (2010). X-ray  
453 tomography measurements of power-law cluster size distributions for the  
454 nonwetting phase in sandstones. *Physical Review E*, 82(5), 056315. doi:  
455 10.1103/PhysRevE.82.056315
- 456 Iglauer, S., Fernø, M. A., Shearing, P., & Blunt, M. J. (2012). Comparison of  
457 residual oil cluster size distribution, morphology and saturation in oil-wet  
458 and water-wet sandstone. *Journal of Colloid and Interface Science*, 375(1),  
459 187–192. doi: 10.1016/j.jcis.2012.02.025
- 460 Jiménez-Martínez, J., de Anna, P., Tabuteau, H., Turuban, R., Borgne, T. L., &  
461 Méheust, Y. (2015). Pore-scale mechanisms for the enhancement of mixing in  
462 unsaturated porous media and implications for chemical reactions. *Geophysical*  
463 *Research Letters*, 42(May), 5316–5324. doi: 10.1002/2015GL064513
- 464 Jiménez-Martínez, J., Le Borgne, T., Tabuteau, H., & Méheust, Y. (2017). Impact  
465 of saturation on dispersion and mixing in porous media: Photobleaching pulse  
466 injection experiments and shear-enhanced mixing model. *Water Resources*  
467 *Research*, 53(2), 1457–1472. doi: 10.1002/2016WR019849
- 468 Kang, P. K., de Anna, P., Nunes, J. P., Bijeljic, B., Blunt, M. J., & Juanes, R.  
469 (2014). Pore-scale intermittent velocity structure underpinning anomalous  
470 transport through 3-D porous media. *Geophysical Research Letters*, 41(17),  
471 6184–6190. doi: 10.1002/2014GL061475
- 472 Kazemifar, F., Blois, G., Kyritsis, D. C., & Christensen, K. T. (2016). Quantify-

- 473 ing the flow dynamics of supercritical CO<sub>2</sub>water displacement in a 2D porous  
 474 micromodel using fluorescent microscopy and microscopic PIV. *Advances in*  
 475 *Water Resources*, *95*, 352–368. doi: 10.1016/j.advwatres.2015.05.011
- 476 Lahav, O., Kochva, M., & Tarchitzky, J. (2010). Potential drawbacks associated  
 477 with agricultural irrigation with treated wastewaters from desalinated water  
 478 origin and possible remedies. *Water Science and Technology*, *61*(10), 2451–  
 479 2460. doi: 10.2166/wst.2010.157
- 480 Le Borgne, T., Bolster, D., Dentz, M., de Anna, P., & Tartakovsky, A. (2011).  
 481 Effective pore-scale dispersion upscaling with a correlated continuous time  
 482 random walk approach. *Water Resources Research*, *47*(12), 1–10. doi:  
 483 10.1029/2011WR010457
- 484 Morales, V. L., Dentz, M., Willmann, M., & Holzner, M. (2017). Stochastic dy-  
 485 namics of intermittent pore-scale particle motion in three-dimensional porous  
 486 media: Experiments and theory. *Geophysical Research Letters*, *44*, 9361–9371.  
 487 doi: 10.1002/2017GL074326
- 488 Moroni, M., Kleinfelter, N., & Cushman, J. H. (2007). Analysis of disper-  
 489 sion in porous media via matched-index particle tracking velocimetry ex-  
 490 periments. *Advances in Water Resources*, *30*(1), 1–15. doi: 10.1016/  
 491 j.advwatres.2006.02.005
- 492 Nützmann, G., Maciejewski, S., & Joswig, K. (2002). Estimation of water satu-  
 493 ration dependence of dispersion in unsaturated porous media: experiments  
 494 and modelling analysis. *Advances in Water Resources*, *25*, 565–576. doi:  
 495 10.1016/S0309-1708(02)00018-0
- 496 Padilla, I. Y., Yah, T.-C. J., & Conklin, M. H. (1999). The effect of water content  
 497 on solute transport in unsaturated porous media. *Water Resources Research*,  
 498 *35*(11), 3303–3313. doi: 10.1029/1999WR900171
- 499 Panfilov, M. (2010). Underground storage of hydrogen: In situ self-organisation and  
 500 methane generation. *Transport in Porous Media*, *85*(3), 841–865. doi: 10.1007/  
 501 s11242-010-9595-7
- 502 Raouf, A., & Hassanizadeh, S. M. (2013). Saturation-dependent solute dispersivity  
 503 in porous media: Pore-scale processes. *Water Resources Research*, *49*(4), 1943–  
 504 1951. doi: 10.1002/wrcr.20152
- 505 Scheffer, K., Méheust, Y., Carvalho, M. S., Mauricio, M. H., & Paciornik, S. (2021).  
 506 Enhancement of oil recovery by emulsion injection: A pore scale analysis from  
 507 X-ray micro-tomography measurements. *Journal of Petroleum Science and*  
 508 *Engineering*, *198*. doi: 10.1016/j.petrol.2020.108134
- 509 Sebilo, M., Mayer, B., Nicolardot, B., Pinay, G., & Mariotti, A. (2013). Long-  
 510 term fate of nitrate fertilizer in agricultural soils. *Proceedings of the National*  
 511 *Academy of Sciences*, *110*(45), 18185–18189. doi: 10.1073/pnas.1305372110
- 512 Stoop, N., Waisbord, N., Kantsler, V., Heinonen, V., Guasto, J. S., & Dunkel,  
 513 J. (2019). Disorder-induced topological transition in porous media flow  
 514 networks. *Journal of Non-Newtonian Fluid Mechanics*, *268*, 66–74. doi:  
 515 10.1016/j.jnnfm.2019.05.002
- 516 Tallakstad, K. T., Løvoll, G., Knudsen, H. A., Ramstad, T., Flekkøy, E. G., &  
 517 Måløy, K. J. (2009). Steady-state, simultaneous two-phase flow in porous  
 518 media: An experimental study. *Physical Review E*, *80*(3), 036308. doi:  
 519 10.1103/PhysRevE.80.036308
- 520 Tang, J., Smit, M., Vincent-Bonnieu, S., & Rossen, W. R. (2019). New Capillary  
 521 Number definition for micromodels: The impact of pore microstructure. *Water*  
 522 *Resources Research*, *55*(2), 1167–1178. doi: 10.1029/2018WR023429
- 523 Vanderborght, J., & Vereecken, H. (2007). Review of dispersivities for transport  
 524 modeling in soils. *Vadose Zone Journal*, *6*(1), 29–52. doi: 10.2136/vzj2006  
 525 .0096
- 526 Whitaker, S. (1986). Flow in porous media I: A theoretical derivation of Darcy’s  
 527 law. *Transport in Porous Media*, *1*(1), 3–25. doi: 10.1007/BF01036523

- 528 Wildenschild, D., & Jensen, K. H. (1999). Laboratory investigations of effective  
529 flow behavior in unsaturated heterogeneous sands. *Water Resources Research*,  
530 *35*(1), 17–27. doi: 10.1029/98WR01958  
531 Winograd, I. (1981). Radioactive waste disposal in thick unsaturated zones. *Science*,  
532 *212*(4502), 1457–1464. doi: 10.1126/science.215.4535.914-c

Accepted Article